Scaling function and nucleon momentum distribution

J. A. Caballero,[1,*] M. B. Barbaro,[2] A. N. Antonov,[3] M. V. Ivanov,[3] and T. W. Donnelly[4]

[1]*Departamento de Física Atómica, Molecular y Nuclear, Universidad de Sevilla, ES-41080 Sevilla, Spain*

[2]*Dipartimento di Fisica Teorica, Università di Torino and INFN, Sezione di Torino, Via P. Giuria 1, I-10125 Torino, Italy*

[3]*Institute for Nuclear Research and Nuclear Energy, Bulgarian Academy of Sciences, BG-1784 Sofia, Bulgaria*

[4]*Center for Theoretical Physics, Laboratory for Nuclear Science and Department of Physics, Massachusetts Institute of Technology, Cambridge, Massachusetts 02139, USA*

(Received 10 March 2010; published 18 May 2010)

Scaling studies of inclusive quasielastic electron scattering reactions have been used in the past as a basic tool to obtain information on the nucleon momentum distribution in nuclei. However, the connection between the scaling function, extracted from the analysis of cross-section data, and the spectral function only exists assuming very restricted approximations. We revisit the basic expressions involved in scaling studies and how they can be linked to the nucleon momentum distribution. In particular, the analysis applied in the past to the so-called scaling region, that is, negative values of the scaling variable y, is extended here to positive y, as a "universal" superscaling function has been extracted from the analysis of the separated longitudinal data. This leads to results that clearly differ from those based solely on the negative-y scaling region, providing new information on how the energy and momentum are distributed in the spectral function.

DOI: 10.1103/PhysRevC.81.055502 PACS number(s): 25.30.Fj, 21.60.Cs, 24.10.Jv, 21.10.Ft

I. INTRODUCTION: BASIC ASPECTS OF SCALING

Scaling studies of inclusive quasielastic (QE) electron-nucleus scattering have largely been considered to provide a powerful tool for extracting the momentum distribution of nucleons inside nuclei [1–7]. Such analyses have been applied to few-body systems, complex nuclei, and nuclear matter, with an important effort devoted to estimating binding corrections and, in particular, the high-momentum components of the nucleon momentum distribution that are governed by short-range correlations [8,9]. However, caution should be borne in mind for the conclusions reached, as a close relationship between the momentum distribution and the scaling function only emerges after some approximations are made. These are linked not only to the general description of the electron scattering reaction mechanism, but also to the integration limits involved and the behavior of the spectral function [1].

The phenomenon of y scaling emerges from the analysis of QE (e,e') reactions. The scaling function, defined as the QE (e,e') differential cross section divided by an appropriate factor involving the single-nucleon cross section [1,10–12], is shown to depend only on a single variable, y, given as a particular combination of the two independent variables in the process, namely, the energy and momentum transfers, ω and q. In the QE domain and for values of ω and q large enough, the basic mechanism in (e,e') reactions on nuclei corresponds to elastic scattering from individual nucleons in the nuclear medium with "quasifree" ejection of a nucleon from the nuclear system. This implies that the inclusive (e,e') cross section is mainly constructed from the exclusive $(e,e'N)$ process, including the contribution of all nucleons in the target and integrating over all (unobserved) ejected nucleon variables. In other words, QE scattering off a nucleus is simply described as an incoherent sum of single-nucleon scattering processes. This approach, which constitutes the basis of the impulse approximation (IA), although being an oversimplified description of (e,e') reactions, has demonstrated its validity under appropriate kinematic conditions. Mechanisms beyond the IA (correlations, meson exchange currents, rescattering processes, etc.) may play a significant role in electron scattering and, hence, may lead to non-negligible scaling violations.

The IA provides an intuitive explanation of how the scaling behavior emerges from the analysis of data. In this case the QE (e,e') cross section is given by

$$\left[\frac{d\sigma}{d\epsilon' d\Omega'}\right]_{(e,e')} = \sum_{i=1}^{A} \int\int_{\Sigma(\omega,q)} p\, dp\, d\mathcal{E} \int d\phi_{N_i} \left(\frac{E_{N_i}}{q p_{N_i}^2}\right) \times \left[\frac{d\sigma}{d\epsilon' d\Omega' dp_{N_i} d\Omega_{N_i}}\right]_{(e,e'N_i)}, \quad (1)$$

where the sum extends to all nucleons in the target and $\{\epsilon', \Omega'\}$ refer to the scattered electron variables. The integration over the ejected (unobserved) nucleon variables $\{p_{N_i}, E_{N_i}, \Omega_{N_i}\}$ has been expressed in terms of the excitation energy $\mathcal{E}$ of the residual nucleus and the missing momentum p. The significance of these variables as well as the kinematically allowed integration region denoted $\Sigma(\omega, q)$ is discussed in detail in next section.

Within the IA, evaluation of $(e,e'N_i)$ cross sections for both proton and neutron knockout determines the inclusive QE cross section. The study of exclusive $(e,e'N)$ reactions has been presented in previous work [13–18], focusing on different aspects of the problem: final-state interactions (FSIs), relativity, correlations, etc. Although such ingredients have been proven to be essential to fit experimental $(e,e'N)$ cross sections, in what follows we restrict our attention to the plane-wave IA (PWIA), where the knocked-out nucleon has no interaction with the residual nucleus. Being the simplest

*jac@us.es

approach to $(e,e'N)$ processes, PWIA retains important relativistic effects that are essential in describing reactions at high q and ω. Moreover, the $(e,e'N)$ differential cross section in PWIA factorizes in two basic terms: the electron-nucleon cross section for a moving, off-shell nucleon and the spectral function that gives the combined probability of finding a nucleon of certain momentum and energy in the nucleus [16–18]. In general we can write

$$\left[\frac{d\sigma}{d\epsilon' d\Omega' dp_N d\Omega_N}\right]^{\rm PWIA}_{(e,e'N)} = K\sigma^{eN}(q,\omega;p,\mathcal{E},\phi_N)S(p,\mathcal{E}), \tag{2}$$

with K a kinematical factor [19] and where p is the missing momentum and $\mathcal{E}$ the excitation energy, essentially the missing energy minus the separation energy. It is important to point out that the factorization property shown in Eq. (2) no longer persists if dynamical relativistic effects in the bound nucleons are incorporated, that is, effects from the lower components in the relativistic wave functions, even in the plane-wave limit [20,21]. Note that both the eN cross section and the spectral function depend on the two integration variables in Eq. (1), p and $\mathcal{E}$. To show how the scaling function emerges from PWIA, further assumptions are needed. First, the spectral function is assumed to be isospin independent, and second, σ^{eN} is assumed to have a very mild dependence on the missing momentum and excitation energy, which is supported by the most commonly used off-shell cross sections [1]. Hence the eN cross section can be evaluated at fixed values of p and $\mathcal{E}$: typically the differential cross section for inclusive QE (e,e') processes is written in the form

$$\left[\frac{d\sigma}{d\epsilon' d\Omega'}\right]_{(e,e')} \cong \overline{\sigma}^e(q,\omega;p=|y|,\mathcal{E}=0)\cdot F(q,\omega)\,, \tag{3}$$

where the single-nucleon cross section is evaluated at the special kinematics $p=|y|$ (with y the scaling variable; see the next section) and $\mathcal{E}=0$ (the residual nucleus in its ground state). This corresponds to the lowest value of the missing momentum occurring when $\mathcal{E}=0$. The term $\overline{\sigma}^e$ refers to the azimuthal-angle-averaged single-nucleon cross section and it also incorporates the kinematical factor K in Eq. (2) and the contribution of all nucleons in the target, that is, $\overline{\sigma}^e \equiv K\sum_{i=1}^{A}\int d\phi_{N_i}\sigma^{eN_i}/2\pi$.

The function $F(q,\omega)$ in Eq. (3) is known as the scaling function and it is given in PWIA in terms of the spectral function:

$$F(q,\omega) = 2\pi\int\!\!\int_{\Sigma(q,\omega)} p\,dp\,d\mathcal{E}\;S(p,\mathcal{E})\,. \tag{4}$$

A detailed study of the scaling function and its connection with the momentum distribution is presented in the next section. However, let us start by pointing out some general interesting features of this basic result. First, only in the case in which it was possible to extend the kinematically allowed region $\Sigma(q,\omega)$ to infinity in the excitation energy plane, that is, $\mathcal{E}_{\rm max}\to\infty$, would the scaling function be directly linked to the true momentum distribution of the A-nuclear system:

$$n(p) \equiv \int_0^\infty d\mathcal{E}\,S(p,\mathcal{E}). \tag{5}$$

Second, guided by the PWIA result in Eq. (3), an experimental scaling function can also be defined by dividing the experimental QE (e,e') cross section by the single-nucleon function, $\overline{\sigma}^e$. At high enough values of the momentum transfer q, the function $F_{\rm exp}(q,\omega)$ has been shown to satisfy scaling in the region below the QE peak; that is, $F_{\rm exp}$ becomes only a function of the scaling variable y (see Refs. [1,11,12], and [22] for details). Note that Eq. (4) does not apply to $F_{\rm exp}(q,\omega)$, which incorporates ingredients not included in the simple PWIA approach: FSIs, meson exchange currents, rescattering processes, etc. The contribution of these effects and their impact on the scaling phenomenon depend on the kinematical region explored, leading, in particular, to a significant scaling breaking in the region above the QE peak.

Furthermore, based on the analysis performed with the relativistic Fermi gas (RFG) model, and making use of the separate longitudinal (L) and transverse (T) (e,e') data, experimental superscaling functions have been introduced:

$$f_{\rm exp}(q,\omega) \equiv k_F F_{\rm exp}(q,\omega), \tag{6}$$

$$f^{L(T)}_{\rm exp}(q,\omega) \equiv k_F F^{L(T)}_{\rm exp}(q,\omega), \tag{7}$$

where k_F is the Fermi momentum. In particular, the L response is thought to have very little contribution from meson production and from meson-exchange currents and thus should be the place where the underlying nuclear dynamics can cleanly be resolved. It has been shown to superscale; that is, the function $f^L_{\rm exp}$ shows only a very mild dependence on the momentum transfer q (first-kind scaling) and the nuclear system considered (second-kind scaling). This has led to the introduction of a universal experimental superscaling function that constitutes a strong constraint for any theoretical model describing QE electron scattering. Not only should the superscaling behavior be fulfilled, but also the specific shape of $f^L_{\rm exp}$ must be reproduced. This subject has been studied in detail in previous work showing the importance of FSI and relativity [23–27], and those studies clearly show that any conclusion about the momentum distribution based on Eq. (4) should be made with caution. Being aware of this, it is illustrative, however, to analyze in detail the basic approaches on which the "link" between the momentum distribution and the scaling (superscaling) function is based. Moreover, the usual analysis, restricted in the past to the region below the QE peak, is now extended to the region above the peak, as the superscaling function $f^L_{\rm exp}$ is defined for both negative and positive values of the scaling variable (see discussion in the next section).

II. THE SCALING FUNCTION

As already shown, in PWIA the scaling function can be expressed as an integral of the spectral function S in the $(p,\mathcal{E})$ plane [Eq. (4)], with p the struck nucleon's momentum,

$$\mathcal{E}(p) \equiv \sqrt{M_B^{*2}+p^2} - \sqrt{M_B^{0^2}+p^2} \geqslant 0 \tag{8}$$

the excitation energy of the recoiling system B, M_B^0 the ground-state mass of the residual nucleus, and M_B^* the general invariant mass of the daughter final state. The integration in Eq. (4) is extended to the kinematically allowed region in

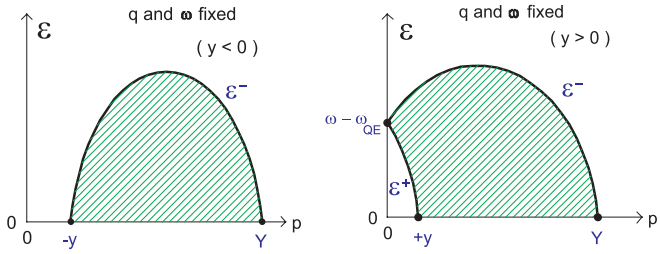

FIG. 1. (Color online) Excitation energy corresponding to negative (left) and positive (right) values of y.

the $(p, \mathcal{E})$ plane at fixed values of the momentum and energy transfer, (q, ω). This is represented by $\Sigma(q, \omega)$. The general kinematics corresponding to QE (e,e') processes leads to the $\mathcal{E}$-integration range [1,10]

$$\max\{0, \mathcal{E}^+\} \leqslant \mathcal{E} \leqslant \mathcal{E}^-, \tag{9}$$

where

$$\mathcal{E}^{\pm}(p; q, \omega) = \left(M_A^0 + \omega\right) - \left[\sqrt{(q \pm p)^2 + m_N^2} + \sqrt{M_B^{0^2} + p^2}\right] \tag{10}$$

and where M_A^0 is the target nuclear mass and m_N the nucleon mass.

The intercepts between the curve $\mathcal{E}^-$ and the p axis are denoted $-y$ and Y; that is, $\mathcal{E}^-(-y; q, \omega) = \mathcal{E}^-(Y; q, \omega) = 0$. The integration region $\Sigma(q, \omega)$ is shown in Fig. 1 for fixed values of the transferred energy and momentum for $\omega < \omega_{\rm QE}$ (left) and $\omega > \omega_{\rm QE}$ (right), with $\omega_{\rm QE}$ the energy at which the quasielastic peak (QEP) occurs. In the region below the QEP, y is negative and $p = -y$ represents the minimum value for the struck nucleon's momentum. Above the QEP y is positive and the curve $\mathcal{E}^+$ cuts the integration region when $p < y$.

In terms of the independent variables q and ω, the intercepts $\pm y$ and Y are given by

$$y(q, \omega) = \left\{\left(M_A^0 + \omega\right)\sqrt{\Lambda^2 - M_B^{0^2} W^2} - q\Lambda\right\}/W^2, \tag{11}$$

$$Y(q, \omega) = \left\{\left(M_A^0 + \omega\right)\sqrt{\Lambda^2 - M_B^{0^2} W^2} + q\Lambda\right\}/W^2, \tag{12}$$

with $W \equiv \sqrt{(M_A^0 + \omega)^2 - q^2}$ the center-of-mass energy and $\Lambda \equiv (M_B^{0^2} - m_N^2 + W^2)/2$. Then the scaling function in Eq. (4) can be recast as follows:

$$\frac{1}{2\pi} F(q, y) = \int_{-y}^{Y(q,y)} p dp \int_0^{\mathcal{E}^-(p;q,y)} d\mathcal{E}\, S(p, \mathcal{E}) \quad \text{if} \quad y < 0, \tag{13}$$

$$\frac{1}{2\pi} F(q, y) = \int_0^{y} p dp \int_{\mathcal{E}^+(p;q,y)}^{\mathcal{E}^-(p;q,y)} d\mathcal{E}\, S(p, \mathcal{E}) + \int_y^{Y(q,y)} p dp \times \int_0^{\mathcal{E}^-(p;q,y)} d\mathcal{E}\, S(p, \mathcal{E}) \quad \text{if} \quad y > 0, \tag{14}$$

for negative and positive values of y, respectively. The analysis presented in the previous work has been restricted to the negative-y region, that is, below the QEP, as this is the region where cross-section data fulfill y-scaling properties. The function $F_{\rm exp}$ does not scale for positive values of y because of the significant scaling violations introduced by effects beyond the IA, namely, inelastic processes and contributions from meson-exchange currents. However, these contributions mostly reside in the purely transverse response and are negligible in the L channel. The "universal" superscaling function extracted from the analysis of the separated L data, and defined for both negative and positive values of the scaling variable, explains our interest in extending the study to the region above the QEP. This strategy, which forces us to employ the superscaling function $f_{\rm exp}^L$ to determine $F_{\rm exp}^L = f_{\rm exp}^L/k_F$ instead of the usual y-scaling function $F_{\rm exp}$, can lead to significant effects concerning the momentum and energy distribution in the spectral function, as discussed here.

In the preceding expressions we have chosen $(p, \mathcal{E}; q, y)$ as independent variables. In terms of these we can also express the energy transfer,

$$\omega(q, y) = \sqrt{(q + y)^2 + m_N^2} + \sqrt{M_B^{0^2} + y^2} - M_A^0, \tag{15}$$

the limits of the excitation energy,

$$\mathcal{E}^{\pm}(p; q, y) = \left[\sqrt{(q + y)^2 + m_N^2} - \sqrt{(q \pm p)^2 + m_N^2}\right] + \left[\sqrt{M_B^{0^2} + y^2} - \sqrt{M_B^{0^2} + p^2}\right], \tag{16}$$

and the upper limit of p,

$$Y(q, y) = \frac{M_B^{0^2}(2q + y) + 2(q + y)\sqrt{M_B^{0^2} + y^2}\sqrt{(q + y)^2 + m_N^2} + y\left[2(q + y)^2 + m_N^2\right]}{M_B^{0^2} + 2\sqrt{M_B^{0^2} + y^2}\sqrt{(q + y)^2 + m_N^2} + 2y(q + y) + m_N^2}. \tag{17}$$

In the thermodynamic limit $M_B^0 \to \infty$, we get

$$\mathcal{E}^{\pm}(p; q, y) \to \sqrt{(q + y)^2 + m_N^2} - \sqrt{(q \pm p)^2 + m_N^2} \equiv E_{q+y} - E_{q\pm p}, \tag{18}$$

$$Y(q, y) \to 2q + y, \tag{19}$$

where we have introduced the nucleon energies $E_k \equiv \sqrt{k^2 + m_N^2}$. Moreover, note that in the limit of a very high momentum transfer, that is, $q \gg |y|$ and $q \gg m_N$, the preceding limiting values reduce to $Y \to 2q$ and $\mathcal{E}^{\pm} \to y \mp p$.

Following previous arguments presented in Refs. [1] and [4], it is instructive to split the spectral function into two

terms, corresponding to zero and finite excitation energy, respectively:

$$S(p,\mathcal{E}) = n_0(p)\delta(\mathcal{E}) + S_1(p,\mathcal{E}), \tag{20}$$

with $S_1(p,\mathcal{E}=0)=0$, which, inserted into Eqs. (13) and (14), yields

$$\frac{1}{2\pi}F(q,y<0) = \int_{-y}^{Y(q,y)} pdp\, n_0(p) + \int_{-y}^{Y(q,y)} p\,dp \times \int_0^{\mathcal{E}^-(p;q,y)} d\mathcal{E}\, S_1(p,\mathcal{E}), \tag{21}$$

$$\frac{1}{2\pi}F(q,y>0) = \int_{y}^{Y(q,y)} pdp n_0(p) + \left[\int_0^{y} pdp \int_{\mathcal{E}^+(p;q,y)}^{\mathcal{E}^-(p;q,y)} d\mathcal{E} + \int_{y}^{Y(q,y)} pdp \int_0^{\mathcal{E}^-(p;q,y)} d\mathcal{E}\right] S_1(p,\mathcal{E}). \tag{22}$$

To analyze how the scaling function and the nucleon momentum distribution are connected, we proceed by evaluating the derivatives of the scaling function F with respect to y and q. Making use of Leibniz's formula and choosing $(p;q,y)$ as the three remaining independent variables, after some algebra we finally get the following results.

A. Negative-y region

$$\frac{1}{2\pi}\frac{\partial F}{\partial y} = Y\, n_0(Y)\left(\frac{\partial Y}{\partial y}\right) - y\, n_0(-y) + \int_{-y}^{Y} p\,dp \left(\frac{\partial \mathcal{E}^-}{\partial y}\right) S_1(p,\,\mathcal{E}^-), \tag{23}$$

$$\frac{1}{2\pi}\frac{\partial F}{\partial q} = Y n_0(Y)\left(\frac{\partial Y}{\partial q}\right) + \int_{-y}^{Y} p\,dp \left(\frac{\partial \mathcal{E}^-}{\partial q}\right) S_1(p,\,\mathcal{E}^-). \tag{24}$$

Making use of the limits in Eq. (16) and assuming the residual mass M_B^0 to be much larger than the momenta, $|y|$, p, q, we simply have

$$\frac{\partial \mathcal{E}^-}{\partial y} \simeq \frac{q+y}{E_{q+y}}, \quad \frac{\partial \mathcal{E}^-}{\partial q} \simeq \frac{q+y}{E_{q+y}} - \frac{q-p}{E_{q-p}}. \tag{25}$$

Likewise, the derivatives of Y reduce to $\partial Y/\partial y \simeq 1$ and $\partial Y/\partial q \simeq 2$.

Introducing these results in the general expressions in Eqs. (23) and (24), we get

$$\frac{1}{2\pi}\frac{\partial F}{\partial y} = Y\, n_0(Y) - y\, n_0(-y) + \frac{q+y}{E_{q+y}} \int_{-y}^{Y} p\,dp\, S_1(p,\,\mathcal{E}^-), \tag{26}$$

$$\frac{1}{2\pi}\frac{\partial F}{\partial q} = 2Y n_0(Y) + \int_{-y}^{Y} p\,dp \times \left[\frac{q+y}{E_{q+y}} - \frac{q-p}{E_{q-p}}\right] S_1(p,\,\mathcal{E}^-), \tag{27}$$

with $\mathcal{E}^-$ and Y given in the thermodynamic limit by Eqs. (18) and (19). Note that the excited-state contribution in the spectral function, that is, S_1, is evaluated at energies along the curve $\mathcal{E}^-$.

For q sufficiently large, $q \gg -y$, the upper limit Y can be safely taken to ∞, and as $\lim_{Y\to\infty} Y n_0(Y) = 0$, the expressions for the derivatives simplify to

$$\frac{1}{2\pi}\frac{\partial F}{\partial y} = -y\, n_0(-y) + \frac{q+y}{E_{q+y}} \int_{-y}^{\infty} p\,dp\, S_1(p,\,\mathcal{E}^-), \tag{28}$$

$$\frac{1}{2\pi}\frac{\partial F}{\partial q} = \int_{-y}^{\infty} p\,dp \left(\frac{q+y}{E_{q+y}} - \frac{q-p}{E_{q-p}}\right) S_1(p,\,\mathcal{E}^-). \tag{29}$$

If we further assume that S_1 is small for large values of p, so that the main contribution to the integral Eq. (29) comes from $p \simeq -y$, then we get

$$\lim_{q\to\infty} \frac{\partial F}{\partial q} = 0, \tag{30}$$

namely, scaling of the first kind (the scaling function F loses its dependence on q).

We also observe that, because at a fixed value of y the integration region in Eq. (27) increases with q and the integrand is a positive function, the asymptotic value $F(y)$ is reached from below (i.e., monotonically increasing as a function of q) in any PWIA approach, in contrast with what experimental data seem to indicate [11,12,22]. This is clearly illustrated in Fig. 2, where the integration region is shown for different values of the momentum transfer at fixed y, and it is also consistent with results shown in Figs. 3(a) and 4(a). In Fig. 3 we present the superscaling function $f(\psi)$ evaluated within the framework of the relativistic PWIA (RPWIA) (see Refs. [24] and [25] for details) for different q values and plotted

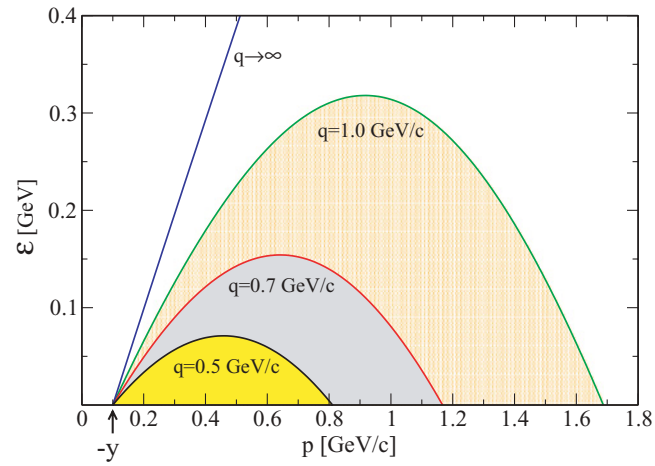

FIG. 2. (Color online) Integration region in the $(\mathcal{E}, p)$ plane for $y = -0.1$ GeV/c and ^{12}C as the target selected. Each curve corresponds to $\mathcal{E}^-$ for a different momentum transfer.

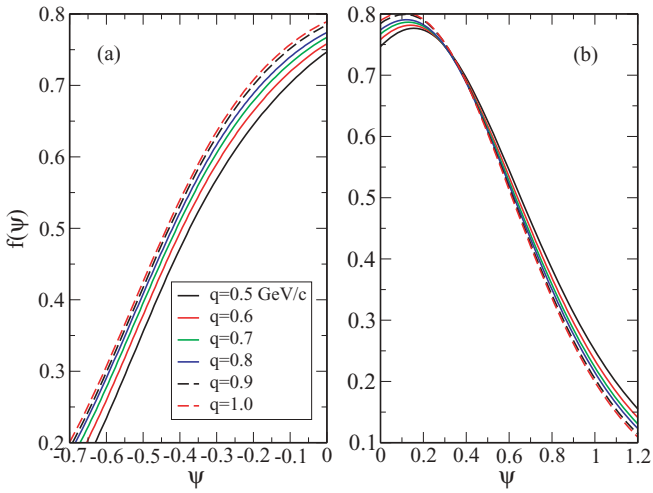

FIG. 3. (Color online) Superscaling function $f(\psi)$ for negative (a) and positive (b) values of the scaling variable ψ. Results correspond to ^{12}C(e,e') evaluated in RPWIA for different momentum transfers.

against the superscaling variable ψ in the negative-ψ region (below the QEP). This variable is given by [10,12]

$$\psi = \frac{1}{\sqrt{\xi_F}} \frac{\lambda - \tau}{\sqrt{(1+\lambda)\tau + \kappa\sqrt{\tau(1+\tau)}}}, \tag{31}$$

where $\lambda \equiv \omega/2m_N$, $\kappa \equiv q/2m_N$, and $\tau \equiv |Q^2|/4m_N^2 = \kappa^2 - \lambda^2$. The scaling variables y and ψ are closely connected [12]:

$$\psi = \left(\frac{y}{k_F}\right)\left[1 + \sqrt{1 + \frac{m_N^2}{q^2}}\frac{1}{2}\eta_F\left(\frac{y}{k_F}\right) + \mathcal{O}\left[\eta_F^2\right]\right] \simeq \frac{y}{k_F}, \tag{32}$$

where $\eta_F = k_F/m_N$, and, as noted above, the superscaling function f is connected to F via $f \equiv k_F \times F$, with k_F the Fermi momentum. The curves in Fig. 3 may be compared with the RPWIA results for the superscaling function, now for negative and positive values of the dimensionless scaling variable y/k_F obtained using the quadratic form of Eq. (32); see Fig. 4. As shown, at fixed ψ (or y/k_F) the function $f(\psi)$ increases with q in accordance with the previous discussion. The basic results shown in Figs. 3 and 4 demonstrate that ψ and y/k_F can be used interchangeably as long as one does not focus on the few percent differences seen in the figures, namely, for large magnitudes of the scaling variables.

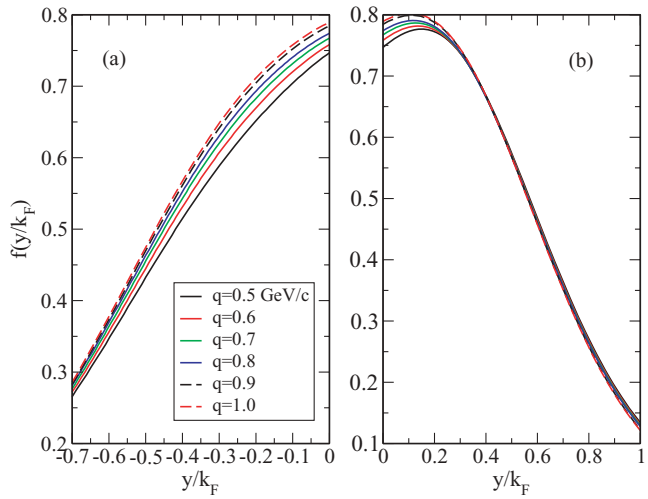

FIG. 4. (Color online) Superscaling function for negative (a) and positive (b) values of the dimensionless scaling variable y/k_F. Results correspond to ^{12}C(e,e') evaluated in RPWIA for different momentum transfers.

In showing the results we choose ^{12}C as an illustrative example. Indeed this nucleus is relevant for many neutrino oscillation experiments, where superscaling ideas can be used to make reliable predictions of neutrino-nucleus cross sections [28]. Moreover, the analysis of the world data performed in Ref. [11] points to an excellent superscaling in the so-called scaling region ($\psi < 0$) for nuclei with $A \geqslant 12$. Note, however, that even the ^{4}He data display a very good superscaling behavior for large negative values of the scaling variable ($\psi < -0.2$), while at the QEP there is a 10% violation owing to the very different spectral function of the lightest nuclei.

B. Positive-y region

In this case, as shown in Fig. 1 (right), the integration region in the $(p, \mathcal{E})$ plane is limited by the two curves, $\mathcal{E}^+$ and $\mathcal{E}^-$, in the missing momentum region $[0, y]$. This makes the derivative analysis somewhat more complicated. Moreover, the experimental data show that scaling arguments of the first kind do not apply to the function $F(q, \omega)$ in this region; that is, F does not become a function dependent only on the scaling variable y. On the contrary, it shows a strong dependence on the momentum transfer q. As already mentioned, this is because of the important contributions beyond the IA contained in the transverse channel. Therefore, although the analysis that follows is applied to $F(q, y)$, it should be clearly stated that only the use of the "universal" (namely, longitudinal) superscaling function f_L, in particular, the study of its derivative with respect to the scaling variable in the positive-y region, can reveal important effects not accounted for by the results obtained in the negative-y scaling region.

After some algebra, the derivatives of the scaling function $F(q, y)$ are given by

$$\frac{1}{2\pi}\frac{\partial F}{\partial y} = Y\, n_0(Y)\left(\frac{\partial Y}{\partial y}\right) - y\, n_0(y) + \int_0^{Y(q,y)} p\, dp\, S_1(p, \mathcal{E}^-)\left(\frac{\partial \mathcal{E}^-}{\partial y}\right) - \int_0^{y} p\, dp\, S_1(p, \mathcal{E}^+)\left(\frac{\partial \mathcal{E}^+}{\partial y}\right), \tag{33}$$

$$\frac{1}{2\pi}\frac{\partial F}{\partial q} = Y n_0(Y)\left(\frac{\partial Y}{\partial q}\right) + \int_0^{Y(q,y)} p\, dp\, S_1(p, \mathcal{E}^-)\left(\frac{\partial \mathcal{E}^-}{\partial q}\right) - \int_0^{y} p\, dp S_1(p, \mathcal{E}^+)\left(\frac{\partial \mathcal{E}^+}{\partial q}\right). \tag{34}$$

As in the previous case, from the general expressions for $\mathcal{E}^{\pm}$ given in Eq. (16) and assuming the thermodynamic limit, we get

$$\frac{\partial \mathcal{E}^{\pm}}{\partial y} \simeq \frac{q+y}{E_{q+y}}, \qquad \frac{\partial \mathcal{E}^{\pm}}{\partial q} \simeq \frac{q+y}{E_{q+y}} - \frac{q \pm p}{E_{q \pm p}}, \tag{35}$$

and the derivatives reduce to

$$\frac{1}{2\pi}\frac{\partial F}{\partial y} = Y\, n_0(Y) - y\, n_0(y) + \frac{q+y}{E_{q+y}} \times \left[\int_0^Y p\, dp\, S_1(p,\, \mathcal{E}^-) - \int_0^y p\, dp\, S_1(p,\, \mathcal{E}^+)\right], \tag{36}$$

$$\frac{1}{2\pi}\frac{\partial F}{\partial q} = 2Y n_0(Y) + \frac{q+y}{E_{q+y}}\left[\int_0^Y p\, dp\, S_1(p,\, \mathcal{E}^-) - \int_0^y p\, dp\, S_1(p,\, \mathcal{E}^+)\right] + \int_0^y p\, dp \frac{q+p}{E_{q+p}} S_1(p,\, \mathcal{E}^+) - \int_0^Y p\, dp \frac{q-p}{E_{q+p}} S_1(p,\, \mathcal{E}^-). \tag{37}$$

Moreover, in the limit of the momentum transfer large enough, $q \gg y$, so that the condition $\lim_{Y\to\infty} Y n_0(Y) = 0$ holds, the expressions of the derivatives result:

$$\frac{1}{2\pi}\frac{\partial F}{\partial y} = -y\, n_0(y) + \frac{q+y}{E_{q+y}}\left[\int_0^\infty p\, dp\, S_1(p,\, \mathcal{E}^-) - \int_0^y p\, dp\, S_1(p,\, \mathcal{E}^+)\right], \tag{38}$$

$$\frac{1}{2\pi}\frac{\partial F}{\partial q} = \int_0^\infty p\, dp \left(\frac{q+y}{E_{q+y}} - \frac{q-p}{E_{q-p}}\right) S_1(p,\, \mathcal{E}^-) - \int_0^y p\, dp \left(\frac{q+y}{E_{q+y}} - \frac{q+p}{E_{q+p}}\right) S_1(p,\, \mathcal{E}^+). \tag{39}$$

Note that in the limit in which y can be neglected compared with q, that is, $(q+y)/E_{q+y} \to q/E_q$, the same comment applies to the ratio $(q+p)/E_{q+p}$ involved in the second integral in Eq. (39), as p is limited within the range $[0, y]$. Thus, in such a limiting case,

$$\int_0^y p\, dp \left(\frac{q+y}{E_{q+y}} - \frac{q+p}{E_{q+p}}\right) S_1(p,\, \mathcal{E}^+) \simeq 0 \quad \text{for} \quad q \gg y, \tag{40}$$

and only the first integral in Eq. (39) survives. Furthermore, if the spectral function is such that we can neglect p compared with q inside the integral, we again get scaling of the first kind: $\lim_{q\to\infty}(\partial F/\partial q) = 0$. This is strictly valid only for very large values of q and it is entirely based on the approximations leading to the expression in Eq. (4) that connects the scaling function to the spectral function. As shown in Fig. 4(b) (positive-y region), the RPWIA scaling function shows a negligible dependence on the momentum transfer for $0.3 \lesssim y/k_F \lesssim 0.8$ ($q \gg y$), whereas for larger y/k_F, scaling of the first kind begins to be slightly violated.

The experimental scaling function extracted from the analysis of data at intermediate q values (less than or of the order of the nucleon mass) shows very important scaling violations in the region above the QEP (positive values of y).

With regard to the dependence of the scaling function F with q at fixed y, we get different behaviors for small and large values of y. Indeed from Eq. (39) we observe that in the case of y being very small (in the vicinity of 0), the second integral in Eq. (39) can be neglected. As the integrand in the remaining integral is positive, we get $\partial F/\partial q > 0$; that is, the scaling function grows with q. This behavior is in accordance with that already shown in the negative-y region. On the contrary, for increasing values of y the first integral in Eq. (39) is expected to diminish significantly, as the excitation energy curve $\mathcal{E}^-$ along which S_1 is evaluated lies much higher than $\mathcal{E}^+$ (see Fig. 5), and it is reasonable to expect that $S_1(p, \mathcal{E})$ gets its main contribution for values of the momentum and energy that are not too large. For y large enough, only the second integral in Eq. (39) survives, and because its integrand is also positive, the minus sign in front of it leads to $\partial F/\partial q < 0$; that is, the scaling function F decreases with q, changing its behavior with respect to the previous cases. It is interesting to point out that this result is consistent with the integration regions shown in Fig. 5 where, for increasing momentum transfer, the curve $\mathcal{E}^+$ moves to higher excitation energies in the $(\mathcal{E}, p)$ plane. This means that as q goes up, regions at low $(\mathcal{E}, p)$ values, where the spectral function mostly resides, are not kinematically accessible anymore. A similar argument can be applied to the case of very small values of y [see Fig. 5(a)]. However, here the integration region lost as $\mathcal{E}^+$ goes up with increasing q is less important than the effects introduced by the growing integration region attached to $\mathcal{E}^-$. This general behavior is also in accordance with the RPWIA results for the superscaling function f shown in Fig. 4(b) (positive values of y), or, alternatively, Fig. 3(b). One sees that f increases with q up to $\psi \gtrsim$

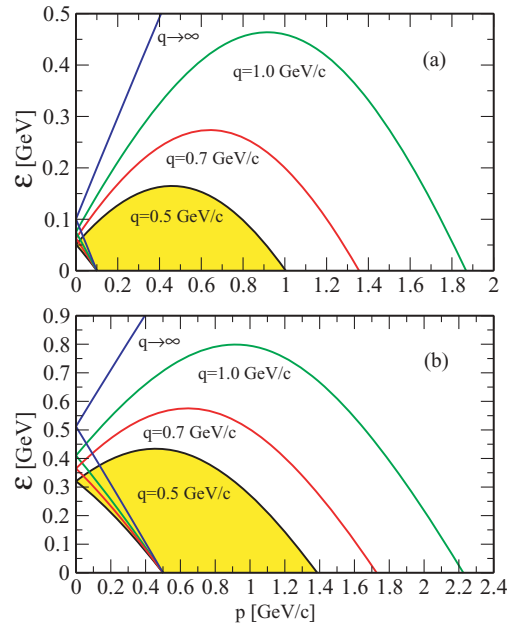

FIG. 5. (Color online) As Fig. 2, but now for positive values of y: (a) $y = 0.1$ GeV/c; (b) $y = 0.5$ GeV/c.

0.4; that is, $y/k_F \sim 0.364$ ($q = 0.5\text{GeV}/c$), $y/k_F \sim 0.375$ ($q = 1.0$ GeV/c), and $y/k_F \sim 0.382$ ($q = \infty\,\text{GeV}/c$), with $k_F = 1.2\,\text{fm}^{-1}$ the Fermi momentum. This corresponds to $y \sim 0.1\,\text{GeV}/c$, which is the situation represented in Fig. 5(a). Also note that the q dependence of f in the region where $y/k_F > 0.3$ shown in Fig. 4 is very weak. Examination of Figs. 5(a) and 5(b) shows that for large y values, the energy curves $\mathcal{E}^{\pm}$ lie very high, and hence, as q increases, the integrals involved incorporate only additional contributions that are very small, leading to a very weak variation with momentum transfer.

III. NUCLEON MOMENTUM DISTRIBUTION AND THE SCALING FUNCTION

In the previous section we have derived general integrodifferential equations connecting the derivatives of the scaling function, $\partial F/\partial y$ and $\partial F/\partial q$, with the spectral function. Based on these results applied to both negative and positive values of y, in what follows we revisit the "usual" procedure to obtain the nucleon momentum distribution function from the analysis of QE (e,e') data. Because the kinematics of electron scattering lead to finite integration limits, we may not a priori draw any strong conclusions about the "true" momentum distribution given as $n(p) \equiv \int_0^\infty d\mathcal{E}\, S(p,\mathcal{E})$, namely, the integral of the spectral function up to infinite excitation energy. However, assuming the spectral function to reside mostly in the $(p,\mathcal{E})$ plane at values of p and $\mathcal{E}$ that are not too large, the previous analyses applied to negative- and positive-y regions lead to different results, thus providing important and complementary information on how the energy and momentum are distributed within the spectral function.

The usual procedure considered in previous work [3,4] to generate the nuclear momentum distribution from the scaling function has been based on the expression

$$n(k) = \left[\frac{-1}{2\pi y}\left(\frac{\partial F}{\partial y}\right)\right]_{|y|=k}, \tag{41}$$

which has been widely applied in the negative-y region. In what follows we extend this study to the positive-y region based on the universal superscaling function introduced from the analysis of the separated longitudinal data.

Making use of the general expressions given by Eqs. (26) and (36) and assuming the limiting case $\lim_{Y\to\infty} Y n_0(Y) = 0$, which is valid if the momentum transfer q is sufficiently large, the momentum distribution functions can be written as follows:

$$\begin{aligned} n^{y<0}(q,k) &= \left[n_0(-y) - \frac{q+y}{yE_{q+y}}\int_{-y}^{\infty} p\,dp S_1(p,\mathcal{E}^-)\right]_{-y=k} \\ &= n_0(k) + \frac{q-k}{kE_{q-k}}\int_k^\infty p\,dp S_1(p,\mathcal{E}^-), \end{aligned} \tag{42}$$

$$\begin{aligned} n^{y>0}(q,k) &= \left[n_0(y) - \frac{q+y}{yE_{q+y}}\left\{\int_0^\infty p\,dp\, S_1(p,\mathcal{E}^-)\right.\right. \\ &\quad \left.\left. - \int_0^y p\,dp S_1(p,\mathcal{E}^+)\right\}\right]_{y=k} = n_0(k) - \frac{q+k}{kE_{q+k}} \\ &\quad \times \left\{\int_0^\infty p\,dp S_1(p,\mathcal{E}^-) - \int_0^k p\,dp S_1(p,\mathcal{E}^+)\right\}. \end{aligned} \tag{43}$$

As observed, both expressions receive contributions from the $A-1$ system ground state, $n_0(k)$, as well as from the excited states described through $S_1(p,\mathcal{E})$. Although using the same notation for the excitation energy $\mathcal{E}^-$, note that the $\mathcal{E}$ curves that enter in the spectral function S_1 in Eqs. (42) and (43) are very different (see Figs. 2 and 5).

Conclusions about the particular behavior of the previous expressions can only be drawn based on a specific model for the spectral function; however, it is illustrative to discuss some general, "model-independent" properties. For negative y the function in Eq. (42) exceeds the purely ground-state contribution, that is, $n^{y<0}(q,k) > n_0(k)$ for all q,k values. This means that the contribution from the excited states adds to the ground-state momentum distribution. Concerning the specific role played by each one of the two terms in Eq. (42), it is difficult to draw stringent conclusions without having control over S_1. As the momentum k grows, the contribution of the integral in Eq. (42) is expected to diminish significantly (S_1 mostly residing at momenta and excitation energies that are not too large). A similar comment also applies to the ground-state contribution, which decreases as k gets larger. The analysis of Eq. (43) in the positive-y region differs because of the relative contributions provided by the two integrals linked to the excited states. In this case the global response $n^{y>0}(q,k)$ can be smaller and/or larger than the purely ground-state contribution, $n_0(k)$, depending on the specific missing momentum value.

In what follows we discuss some particular situations in detail, thereby drawing some preliminary conclusions on the general behavior shown by $n^{y\lessgtr 0}(q,k)$. Let us start by considering the value of the nucleon momentum k to be in the vicinity of 0. Thus, neglecting k compared with the momentum transfer q ($k \ll q$) and assuming $\int_0^\infty p\,dp\, S_1(p,\mathcal{E}^-) \gg \int_0^k p\,dp\, S_1(p,\mathcal{E}^+) \to 0$, we can write

$$n^{y<0}(q,k) \simeq n_0(k) + \frac{q}{kE_q}\int_k^\infty p\,dp\, S_1(p,\mathcal{E}^-) > n_0(k), \tag{44}$$

$$n^{y>0}(q,k) \simeq n_0(k) - \frac{q}{kE_q}\int_0^\infty p\,dp\, S_1(p,\mathcal{E}^-) < n_0(k). \tag{45}$$

From these results the following relation (valid for k small enough) occurs:

$$n^{y>0}(q,k) \leqslant n_0(k) \leqslant n^{y<0}(q,k). \tag{46}$$

Moreover, from Eqs. (44) and (45) the ground-state contribution is roughly given as $n_0(k) \simeq [n^{y<0} + n^{y>0}]/2$.

As the nucleon momentum k grows, the two functions $n^{y<0}(q,k)$ and $n^{y>0}(q,k)$ in Eqs. (42) and (43) get closer, crossing each other at some specific k, such that $n^{y>0}(q,k) > n^{y<0}(q,k)$ for larger k. From the integration region in the $(\mathcal{E}$-$p)$ plane shown in Fig. 5, and assuming most of the strength in the spectral function to be located at not too high p and $\mathcal{E}$, we can conclude that for intermediate to high missing momentum values the main contribution in $n^{y>0}(q,k)$ comes from the second integral in Eq. (43); that is, $n^{y>0}(q,k) \simeq [(q+k)/(kE_{q+k})]\int_0^k p\,dp S_1(p,\mathcal{E}^+)$.

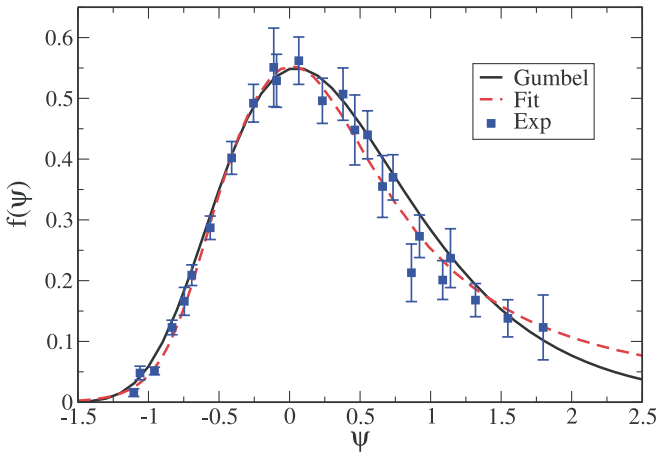

FIG. 6. (Color online) Average $f_L^{\rm exp}(\psi)$ compared with the Gumbel distribution in Eq. (47) (solid curve) and a fit of the experimental data (dashed curve).

To prove these general properties, in what follows we present results based on the derivative analysis making use of the superscaling function $f(\psi)$. To simplify the calculations we represent $f(\psi)$ by means of the Gumbel probability density function (i.e., the derivative of the Gumbel distribution):

$$f_G(\psi) = \frac{1}{\sigma}\exp\left[-\frac{(\psi-\mu)}{\sigma}\right]\exp\left[-\exp\left[-\frac{(\psi-\mu)}{\sigma}\right]\right]. \tag{47}$$

In our case the values of the parameters are $\mu = 0$ and $\sigma = 0.67$ [$f_G^{\rm max} = f_G(0) = 0.55$]. In Fig. 6 we compare the Gumbel distribution [Eq. (47)] with $f_{\rm exp}^L(\psi)$ and a fit of the experimental data [22]. As shown, the Gumbel distribution nicely fits the data. Moreover, it fulfills the unitarity condition $\int_{-\infty}^{+\infty} f(\psi)d\psi = 1$. The nucleon momentum distribution is evaluated through the derivative of the scaling function by using Eq. (41) and recalling that $f = k_F F$, thus getting

$$n(k) = \left[-\frac{1}{2\pi y}\frac{1}{k_F}\frac{df(\psi(y))}{dy}\right]_{|y|=k}, \tag{48}$$

which, using the approximate relation $\psi \simeq y/k_F$, can be presented in the form

$$n(k) = -\frac{1}{2\pi k}\frac{1}{k_F}\left[\frac{df(\psi)}{d(k_F|\psi|)}\right]_{k_F|\psi|=k}. \tag{49}$$

Note that if the superscaling function is not symmetric with respect to ψ, as is the case for the experimental data, Eq. (49) yields different momentum distributions for negative and positive values of ψ, which are denoted $n^<$ and $n^>$, respectively. On the contrary, symmetric scaling functions, like the RFG one, lead to $n^< = n^>$.

In the case of the Gumbel distribution, we get (setting $\mu = 0$)

$$\frac{df_G(\psi)}{d\psi} = \frac{1}{\sigma}(e^{-\psi/\sigma} - 1)f_G(\psi), \tag{50}$$

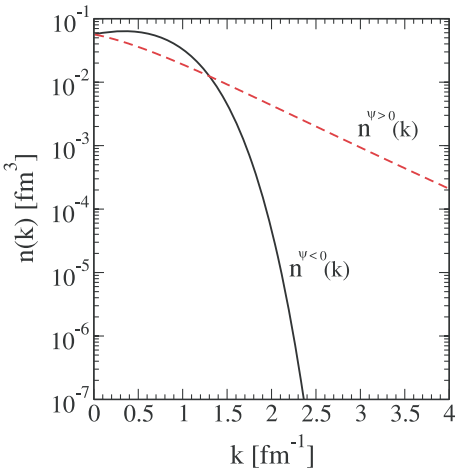

FIG. 7. (Color online) Nucleon momentum distribution extracted through the derivative of the superscaling function given by the Gumbel probability density in Eq. (47). Results corresponding to negative (solid line) and positive (dashed line) values of the scaling variable are compared.

which leads to

$$n_G^<(k) = \frac{1}{2\pi\sigma k_F^2 k}[e^{k/(\sigma k_F)} - 1]f_G(-k/k_F), \tag{51}$$

$$n_G^>(k) = \frac{1}{2\pi\sigma k_F^2 k}[1 - e^{-k/(\sigma k_F)}]f_G(k/k_F). \tag{52}$$

In Fig. 7 we present the results for $n^{\psi<0}(k) = n_G^<(k)/2$ (solid line) and $n^{\psi>0}(k) = n_G^>(k)/2$ (dashed line), with $n_G^<(k)$ and $n_G^>(k)$ given in Eqs. (51) and (52) (at $k_F = 1.2$ fm^{-1}). As expected, $n_G^<(k)$ and $n_G^>(k)$ (and $n^{\psi<0}$ and $n^{\psi>0}$, respectively) coincide in the limiting case $k = 0$:

$$n_G^>(0) = n_G^<(0) = \frac{1}{2\pi\sigma^3 k_F^3 e}. \tag{53}$$

For missing momenta up to $k \sim 1$ fm^{-1} the main contribution resides in $n^<$, which is in accordance with Eq. (46) and the general discussion presented above. At $k \simeq 1.3$–1.4 fm^{-1}, that is, k close to the Fermi momentum, $n^<$ and $n^>$ cross each other, with $n^>$ being much higher for larger k values. In fact, whereas $n^<$ shows a steep slope when k increases, which is in accordance with results based on independent-particle model descriptions, $n^>$ presents a high momentum tail very far from $n^<$ and, hence, from shell-model results (see next section). As already explained, this tail at intermediate to high k is linked to the much larger contribution given by the spectral function S_1 when evaluated along the curve $\mathcal{E}^+$ instead of $\mathcal{E}^-$. This general behavior is illustrated in Fig. 8, where the contour curves $\mathcal{E}^\pm$ corresponding to positive and negative y values are presented. The presence of the tail at high momentum values in the nucleon momentum distribution is a clear signature of the importance of nucleon-nucleon correlations. Because the spectral function maps very different regions in the $(\mathcal{E} - k)$ plane for negative and positive y (Fig. 8), the joint analysis of the two kinematical regions can provide important clues in the knowledge of NN correlations. It should be pointed out that the functions $n^{\psi<0}(k)$ and $n^{\psi>0}(k)$, evaluated through Eq. (49)

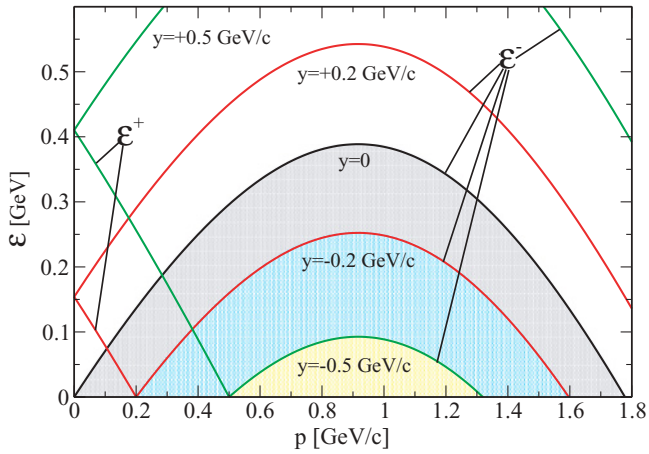

FIG. 8. (Color online) Integration region in the $(\mathcal{E}, p)$ plane for $q = 1$ GeV/c and different, negative and positive, values of the scaling variable y. The contour curves $\mathcal{E}^{\pm}$ in both regions are represented.

and presented in Fig. 7, are normalized to different values connected with the different areas subtended by the Gumbel distribution function $f_G(\psi)$ at negative and positive ψ, that is, 0.37 (for $\psi < 0$) and 0.63 ($\psi > 0$).

In particular, it has been shown in Refs. [24] and [26] in the framework of relativistic nuclear models that the large positive-ψ tail of the scaling function is closely related to FSIs, while the negative-ψ region is more affected by initial-state correlations, as also shown in the next section using the CDFM model. The possibility of connecting different aspects of the momentum distribution to initial- and final-state physics will be explored further in future work.

IV. NUCLEON MOMENTUM DISTRIBUTION WITHIN THE COHERENT DENSITY FLUCTUATION MODEL

In this section we give, as an example, the results for the nucleon momentum distribution extracted from the scaling function, obtained within the framework of a particular nuclear model, namely, the coherent density fluctuation model (CDFM) [29,30]. The latter is a natural extension to finite nuclei of the RFG model within which the scaling variable ψ' was introduced.[1] The CDFM is based on the generator coordinate method [31] and includes long-range NN correlations (LRC) of collective type. In [32,33] the scaling function was defined within the CDFM using the RFG scaling function [10,34–36] and applied it to various processes [32,33,37–40].

In the CDFM model [29,30], the one-body density matrix $\rho(\mathbf{r}, \mathbf{r}')$ is an infinite superposition of one-body density matrices $\rho_x(\mathbf{r}, \mathbf{r}')$ corresponding to single Slater determinant wave functions of systems of A free nucleons homogeneously distributed in a sphere with radius x, density $\rho_0(x) \equiv 3A/(4\pi x^3)$, and Fermi momentum $k_F(x) \equiv [\frac{3\pi^2}{2}\rho_0(x)]^{1/3} \equiv \frac{\alpha}{x}$ [with $\alpha \equiv (\frac{9\pi}{8}A)^{1/3} \cong 1.52A^{1/3}$]:

$$\rho(\mathbf{r}, \mathbf{r}') = \int_0^\infty |F(x)|^2 \rho_x(\mathbf{r}, \mathbf{r}')dx. \tag{54}$$

The weight function $|F(x)|^2$ can be expressed in an equivalent way either by means of the density distribution [29,30,33],

$$|F(x)|^2 = -\frac{1}{\rho_0(x)}\frac{d\rho(r)}{dr}\bigg|_{r=x} \quad \text{at} \quad \frac{d\rho(r)}{dr} \leqslant 0, \tag{55}$$

or by means of the nucleon momentum distribution [33],

$$|F(x)|^2 = -\frac{3\pi^2}{2}\frac{\alpha}{x^5}\frac{dn(k)}{dk}\bigg|_{k=\alpha/x} \quad \text{at} \quad \frac{dn(k)}{dk} \leqslant 0. \tag{56}$$

In Eqs. (55) and (56)

$$\int \rho(\mathbf{r})d\mathbf{r} = A, \quad \int n(\mathbf{k})d\mathbf{k} = A, \quad \int_0^\infty |F(x)|^2 dx = 1. \tag{57}$$

In the version of the CDFM approach suggested in Refs. [32] and [33], the scaling function has the form

$$f(\psi') = \int_0^{\alpha/(k_F|\psi'|)} |F(x)|^2 f_{\rm RFG}(x, \psi')dx, \tag{58}$$

where the RFG scaling function is

$$f_{\rm RFG}(x, \psi') = \frac{3}{4}\left[1 - \left(\frac{k_F x|\psi'|}{\alpha}\right)^2\right] \times \left\{1 + \left(\frac{xm_N}{\alpha}\right)^2\left(\frac{k_F x|\psi'|}{\alpha}\right)^2 \times \left[2 + \left(\frac{\alpha}{xm_N}\right)^2 - 2\sqrt{1 + \left(\frac{\alpha}{xm_N}\right)^2}\right]\right\}. \tag{59}$$

In the CDFM the Fermi momentum k_F is calculated for each nucleus by

$$k_F = \int_0^\infty k_F(x)|F(x)|^2 dx = \int_0^\infty \frac{\alpha}{x}|F(x)|^2 dx \tag{60}$$

and is not a fitting parameter, as it is in the RFG model.

By using Eqs. (55) and (56) in Eqs. (58) and (60), the CDFM scaling function $f(\psi')$ and k_F can be expressed equivalently by the density and momentum distributions [33]:

$$f(\psi') = \frac{4\pi}{A}\int_0^{\alpha/(k_F|\psi'|)} \rho(x)\left[x^2 f_{\rm RFG}(\psi', x) + \frac{x^3}{3}\frac{df_{\rm RFG}(\psi', x)}{dx}\right]dx, \tag{61}$$

where $f_{\rm RFG}(\psi', x)$ is given by Eq. (59), and

$$f(\psi') = \frac{4\pi}{A}\int_{k_F|\psi'|}^\infty n(k)\left[k^2 f_{\rm RFG}(\psi', k) + \frac{k^3}{3}\frac{df_{\rm RFG}(\psi', k)}{dk}\right], \tag{62}$$

[1]The scaling variable ψ' differs from ψ by a phenomenological energy shift $E_s \simeq 20$ MeV (for ^{12}C) introduced to reproduce the experimental position of the QEP: $\psi'(q, \omega) = \psi(q, \omega - E_s)$.

where

$$f_{\rm RFG}(\psi',k)=\frac{3}{4}\left[1-\left(\frac{k_F|\psi'|}{k}\right)^2\right]\left\{1+\left(\frac{m_N}{k}\right)^2\left(\frac{k_F|\psi'|}{k}\right)^2 \times\left[2+\left(\frac{k}{m_N}\right)^2-2\sqrt{1+\left(\frac{k}{m_N}\right)^2}\right]\right\}. \quad (63)$$

Equation (62) is valid under the condition

$$\lim_{k\to\infty}[n(k)k^3]=0. \quad (64)$$

From Eq. (62) one can estimate the possibility of obtaining information about the nucleon momentum distribution from the empirical data for the scaling function. If we keep only the main term of the RFG scaling function from Eq. (63),

$$f_{\rm RFG}(\psi',k)\simeq\frac{3}{4}\left[1-\left(\frac{k_F\psi'}{k}\right)^2\right] \quad (65)$$

and its derivative,

$$\frac{\partial f_{\rm RFG}(\psi',k)}{\partial k}\simeq\frac{3}{2}\frac{(k_F|\psi'|)^2}{k^3}, \quad (66)$$

then

$$f(\psi')\simeq 3\pi\int_{k_F|\psi'|}^{\infty}n(k)k^2\left[1-\frac{1}{3}\frac{(k_F|\psi'|)^2}{k^2}\right]dk. \quad (67)$$

In Eq. (67)

$$\int n(\mathbf{k})d\mathbf{k}=1. \quad (68)$$

Using Eq. (67), $n(k)$ can be found by solving the integral-differential equation:

$$n(k)=-\frac{1}{2\pi k^2}\left.\frac{\partial f(\psi')}{\partial(k_F|\psi'|)}\right|_{k_F|\psi'|=k}-\frac{1}{k}\int_k^{\infty}dk'n(k'). \quad (69)$$

In this work we solve the Eq. (69) from CDFM using the experimentally obtained scaling function. The latter can be represented by the Gumbel probability density function in Eq. (47). The results for the nucleon momentum distribution obtained in this way are shown in Fig. 9 as dashed lines in both cases: $n^<(k)$ for $\psi<0$ (dashed line labeled $n^<_{\rm Gumbel}$) and $n^>(k)$ for $\psi>0$ (dashed line labeled $n^>_{\rm Gumbel}$). They are compared with the results obtained using the expression for $n(k)$ through the derivative of the scaling function, Eq. (49).

The momentum distributions $n^<(k)$ and $n^>(k)$ obtained using Eq. (49) and the experimental scaling function presented by Eq. (47) are given in Fig. 9 as solid lines. For comparison we present in the same figure the momentum distributions from the RFG model ($n_{\rm RFG}$), the shell-model results (using Woods-Saxon single-particle wave functions) for ^{56}Fe ($n_{\rm WS}$), and the momentum distribution ($n_{\rm LFD}$) obtained within the light-front dynamics approach [41] (see also Ref. [33] and the late modification of the approach in Ref. [38]). The latter is based on the nucleon momentum distribution in the deuteron (including its high-momentum component) from the light-front dynamics method (e.g., Refs. [42] and [43], and references therein). In the calculations $k_F=1.2$ fm^{-1}. In Fig. 9 all nucleon momentum distributions are normalized to unity [Eq. (68)].

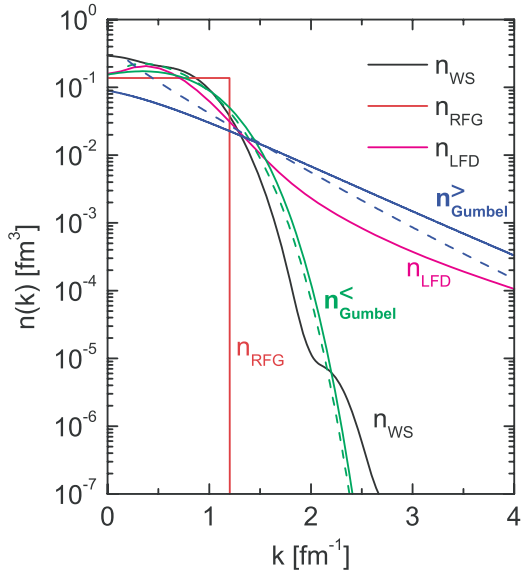

FIG. 9. (Color online) Nucleon momentum distribution extracted from the scaling function. Solid lines: $n^<$ [light (green)] and $n^>$ [dark (blue)] obtained through the derivative of the scaling function [Eq. (49)]. Dashed lines: $n^<$ [light (green)] and $n^>$ [dark (blue)] using the CDFM integral-differential equation [Eq. (69)]. The Gumbel probability density function $f_G(\psi)$ [Eq. (47)] is used in the calculations. For comparison, the momentum distributions from the relativistic Fermi gas model ($n_{\rm RFG}$), from the shell model ($n_{\rm WS}$), and from the light front dynamics ($n_{\rm LFD}$) are given. All momentum distributions are normalized to unity [Eq. (68)].

One can see from Fig. 9 that, in general, the results for $n(k)$ in CDFM confirm the considerations made in Secs. I–III:

(i) At $k\lesssim 1.3$ fm^{-1} the CDFM momentum distributions [from Eq. (69)] $n^<(k)>n^>(k)$, while at $k\gtrsim 1.3$ fm^{-1}, $n^<(k)<n^>(k)$. The same is valid for the momentum distribution obtained using Eq. (49). This is in accord with the general consideration from Sec. III.

(ii) The crossing point of the lines showing $n^<(k)$ and $n^>(k)$ from Eq. (49) is at a slightly smaller value of k than that for $n^<(k)$ and $n^>(k)$ obtained from Eq. (69). This follows also from the comparison of the explicit forms of Eqs. (69) and (49).

(iii) $n^<(k)$ from Eq. (69) is close to the result for $n^<(k)$ from Eq. (49), while the difference between $n^>(k)$ from Eq. (49) and $n^>(k)$ from Eq. (69) increases with k. At $k=4$ fm^{-1}, $n^>(k)$ from Eq. (49) is about twice larger than $n^>(k)$ from Eq. (69). At the same time, for $k\lesssim 1.2$ fm^{-1}, $n^>(k)$ from Eq. (69) is larger than $n^>(k)$ from Eq. (49).

V. CONCLUSIONS

In the present work a study of the scaling function and its connection with the momentum distribution is presented.

As is well known, a close relationship between the two quantities exists using the PWIA and, under some conditions, for the kinematically allowed region [$\Sigma(q,\omega)$], once one has accounted for the roles of FSIs, meson exchange currents, rescattering processes, etc. Here these restricted approximations are considered in detail. The "usual" analyses performed in the past to the region below the QE peak is extended to the region above the peak, as the superscaling function is defined for both negative and positive values of the scaling variable. This is justified, as a "universal" superscaling function has been extracted from the analysis of the separated longitudinal data. The explicit expressions for the derivatives $\partial F/\partial y$ and $\partial F/\partial q$ for both negative- and positive-y regions are derived and their dependences on q and y are analyzed.

The general integrodifferential equations connecting the derivatives $\partial F/\partial y$ and $\partial F/\partial q$ with the spectral function are derived. The results obtained allow us to revisit the "usual" procedure to obtain the nucleon momentum distribution from the analyses of the QE scattering data. The considerations in the present work lead to results that are quite different from those obtained solely in the negative-y scaling region and provide information about the energy and momentum distribution in the spectral function. It is shown that the expressions for the nucleon momentum distributions $n^{y<0}(q,k)$ and $n^{y>0}(q,k)$ have contributions from the momentum distribution $n_0(k)$ of the ground state of the system with $A-1$ nucleons, as well as from the part of the spectral function $S_1(p,\mathcal{E})$ that contains information about the excited states. It is shown that for small momenta k, $n^{y>0}(q,k) \leqq n_0(k) \leqq n^{y<0}(q,k)$, while as k grows the two functions, $n^{y<0}(q,k)$ and $n^{y>0}(q,k)$, get closer, crossing each other at some value of k and yielding $n^{y>0}(q,k) > n^{y<0}(q,k)$ for higher k.

The general properties of the momentum distribution established in the present work are validated by the results obtained from the derivative analysis using the superscaling function $f(\psi)$ represented by the parameterized Gumbel probability density function, which provides a good fit to the experimental longitudinal scaling function $f^L_{\rm exp}(\psi)$. It is concluded that the high-momentum tail of the momentum distribution is a clear signature for the important effects stemming from nucleon-nucleon correlations.

The general properties of the nucleon momentum distribution obtained are also illustrated using the scaling function obtained in the framework of a particular nuclear model, namely, the CDFM, which includes collective long-range NN correlations. It is shown that the momentum distribution in the CDFM has the properties already pointed out in the general consideration.

ACKNOWLEDGMENTS

This work was partially supported by DGI (MICINN-Spain) Contract Nos. FIS2008-04189 and PCI2006-A7-0548, by the Spanish Consolider-Ingenio programme CPAN (Grant No. CSD2007-00042), by the Junta de Andalucía, and by the INFN-CICYT collaboration agreements INFN08-20 and FPA2008-03770-E/INFN, as well as by the Bulgarian National Science Fund under Contract Nos. DO-02-285 and DID-02/16-17.12.2009. M.V.I. acknowledges support from the European Operational programm HRD through Contract No. BGO051PO001/07/3.3-02/53 with the Bulgarian Ministry of Education. This work was also supported in part (T.W.D.) by the US Department of Energy under Cooperative Agreement DE-FC02-94ER40818.

[1] D. B. Day, J. S. McCarthy, T. W. Donnelly, and I. Sick, Annu. Rev. Nucl. Part. Sci. **40**, 357 (1990).
[2] C. Ciofi degli Atti, E. Pace, and G. Salmè, Phys. Rev. C **36**, 1208 (1987).
[3] C. Ciofi degli Atti, E. Pace, and G. Salmé, Phys. Rev. C **39**, 259 (1989).
[4] C. Ciofi degli Atti, E. Pace, and G. Salmé, Phys. Rev. C **43**, 1155 (1991).
[5] C. Ciofi degli Atti, D. B. Day, and S. Liuti, Phys. Rev. C **46**, 1045 (1992).
[6] C. Ciofi degli Atti and S. Simula, Phys. Rev. C **53**, 1689 (1996).
[7] C. Ciofi degli Atti and G. B. West, Phys. Lett. B **458**, 447 (1999).
[8] X. Ji and J. Engel, Phys. Rev. C **40**, 497R (1989).
[9] C. Ciofi degli Atti and C. B. Mezzetti, Phys. Rev. C **79**, 051302 (2009).
[10] W. M. Alberico, A. Molinari, T. W. Donnelly, E. L. Kronenberg, and J. W. Van Orden, Phys. Rev. C **38**, 1801 (1988).
[11] T. W. Donnelly and I. Sick, Phys. Rev. Lett. **82**, 3212 (1999).
[12] T. W. Donnelly and I. Sick, Phys. Rev. C **60**, 065502 (1999).
[13] J. M. Udías, P. Sarriguren, E. Moya de Guerra, E. Garrido, and J. A. Caballero, Phys. Rev. C **48**, 2731 (1993); **51**, 3246 (1995).
[14] J. M. Udías, P. Sarriguren, E. Moya de Guerra, and J. A. Caballero, Phys. Rev. C **53**, 1488R (1996).
[15] J. M. Udías, J. A. Caballero, E. Moya de Guerra, J. R. Vignote, and A. Escuderos, Phys. Rev. C **64**, 024614 (2001).
[16] S. Frullani and J. Mougey, Adv. Nucl. Phys. **14**, 1 (1984).
[17] S. Boffi, C. Giusti, F. D. Pacati, and M. Radici, Phys. Rep. **226**, 1 (1993); *Electromagnetic Response of Atomic Nuclei* (Oxford University Press, Oxford, 1996).
[18] J. J. Kelly, Adv. Nucl. Phys. **23**, 75 (1996).
[19] A. S. Raskin and T. W. Donnelly, Ann. Phys. (NY) **191**, 78 (1989).
[20] J. A. Caballero, T. W. Donnelly, E. Moya de Guerra, and J. M. Udías, Nucl. Phys. A **643**, 189 (1998); **632**, 323 (1998).
[21] M. C. Martínez, J. A. Caballero, and T. W. Donnelly, Nucl. Phys. A **707**, 83 (2002), and references therein.
[22] C. Maieron, T. W. Donnelly, and I. Sick, Phys. Rev. C **65**, 025502 (2002).
[23] J. E. Amaro, M. B. Barbaro, J. A. Caballero, T. W. Donnelly, and C. Maieron, Phys. Rev. C **71**, 065501 (2005).
[24] J. A. Caballero, J. E. Amaro, M. B. Barbaro, T. W. Donnelly, C. Maieron, and J. M. Udías, Phys. Rev. Lett. **95**, 252502 (2005).
[25] J. A. Caballero, Phys. Rev. C **74**, 015502 (2006).
[26] J. E. Amaro, M. B. Barbaro, J. A. Caballero, T. W. Donnelly, and J. M. Udías, Phys. Rev. C **75**, 034613 (2007).
[27] J. A. Caballero, J. E. Amaro, M. B. Barbaro, T. W. Donnelly, and J. M. Udías, Phys. Lett. B **653**, 366 (2007).

[28] J. E. Amaro, M. B. Barbaro, J. A. Caballero, T. W. Donnelly, A. Molinari, and I. Sick, Phys. Rev. C **71**, 015501 (2005).
[29] A. N. Antonov, V. A. Nikolaev, and I. Zh. Petkov, Bulg. J. Phys. **6**, 151 (1979); Z. Phys. A **297**, 257 (1980); **304**, 239 (1982); Nuovo Cimento A **86**, 23 (1985); **102**, 1701 (1989); A. N. Antonov, D. N. Kadrev, and P. E. Hodgson, Phys. Rev. C **50**, 164 (1994).
[30] A. N. Antonov, P. E. Hodgson, and I. Zh. Petkov, *Nucleon Momentum and Density Distributions in Nuclei* (Clarendon Press, Oxford, 1988); *Nucleon Correlations in Nuclei* (Springer-Verlag, Berlin, 1993).
[31] J. J. Griffin and J. A. Wheeler, Phys. Rev. **108**, 311 (1957).
[32] A. N. Antonov, M. K. Gaidarov, D. N. Kadrev, M. V. Ivanov, E. Moya de Guerra, and J. M. Udias, Phys. Rev. C **69**, 044321 (2004).
[33] A. N. Antonov, M. K. Gaidarov, M. V. Ivanov, D. N. Kadrev, E. Moya de Guerra, P. Sarriguren, and J. M. Udias, Phys. Rev. C **71**, 014317 (2005).
[34] M. B. Barbaro, R. Cenni, A. De Pace, T. W. Donnelly, and A. Molinari, Nucl. Phys. A **643**, 137 (1998).
[35] T. W. Donnelly and I. Sick, Phys. Rev. Lett. **82**, 3212 (1999).
[36] T. W. Donnelly and I. Sick, Phys. Rev. C **60**, 065502 (1999).
[37] A. N. Antonov, M. V. Ivanov, M. K. Gaidarov, E. Moya de Guerra, P. Sarriguren, and J. M. Udias, Phys. Rev. C **73**, 047302 (2006).
[38] A. N. Antonov, M. V. Ivanov, M. K. Gaidarov, E. Moya de Guerra, J. A. Caballero, M. B. Barbaro, J. M. Udias, and P. Sarriguren, Phys. Rev. C **74**, 054603 (2006).
[39] M. V. Ivanov, M. B. Barbaro, J. A. Caballero, A. N. Antonov, E. Moya de Guerra, and M. K. Gaidarov, Phys. Rev. C **77**, 034612 (2008).
[40] A. N. Antonov, M. V. Ivanov, M. B. Barbaro, J. A. Caballero, and E. Moya de Guerra, Phys. Rev. C **79**, 044602 (2009).
[41] A. N. Antonov, M. K. Gaidarov, M. V. Ivanov, D. N. Kadrev, G. Z. Krumova, P. E. Hodgson, and H. V. von Geramb, Phys. Rev. C **65**, 024306 (2002).
[42] J. Carbonell and V. A. Karmanov, Nucl. Phys. A **581**, 625 (1995).
[43] J. Carbonell, B. Desplanques, V. A. Karmanov, and J.-F. Mathiot, Phys. Rep. **300**, 215 (1998).